Improvement of Multimodel Ensemble Seasonal Prediction Skills over East Asian Summer Monsoon Region Using a Climate Filter Concept

DOO YOUNG LEE

Asia-Pacific Economic Cooperation Climate Center, and Department of Atmospheric Sciences, Pusan National University, Busan, South Korea

JOONG-BAE AHN

Department of Atmospheric Sciences, Pusan National University, Busan, South Korea

KARUMURI ASHOK

Centre for Climate Change Research, Indian Institute of Tropical Meteorology, Pune, India

ABSTRACT

The authors propose the use of a ''climate filter'' concept to enhance prediction skill of a multimodel ensemble (MME) suite for the East Asian summer monsoon (EASM) precipitation and temperature at 850 hPa. The method envisages grading models on the basis of the degree of reproducibility of the association of EASM variability with a few relevant climate drivers with the respective model hindcasts for the period 1981–2003. The analysis identifies the previous winter Niño-3.4 and spring North Atlantic Oscillation indices as the most suitable climate drivers in designing a climate filter for evaluating models that replicate the observed teleconnections to EASM well. The results show that the hindcast skills of a new MME with the better-performing models are significantly higher than those from the nonperforming models or from an all-inclusive operational MME.

1. Introduction

The summer (June–August) rainfall in East Asia is broadly known as the East Asian summer monsoon (EASM) and involves considerable spatial and subseasonal variation [see Ding and Chan (2005) for details]. The broad spatial distribution of the interannually variable EASM rainfall, presented in Fig. 1a, can be gauged from the gravest mode (obtained by an empirical orthogonal function analysis; Wilks 1995).

Skillful seasonal prediction of the EASM remains an outstanding challenge for research and operations. Interestingly, newer seasonal prediction methods have been introduced in the last decade or so, and these methods hold promise for the general improvement of seasonal prediction. Research in the last decade (e.g., Krishnamurti et al. 1999, 2000; Palmer et al. 2000; Shukla et al. 2000; Doblas-Reyes et al. 2000, 2005; Peng et al. 2002; Barnston et al. 2003; Hagedorn et al. 2005; Yun et al. 2005; Sahai et al. 2008; Wang et al. 2008a, 2009; Lee et al. 2008, 2011) has shown that the multimodel ensemble (MME) approach is an effective method in dynamical climate prediction, in reducing the uncertainty arising from atmospheric or oceanic model dynamics and from physical parameterizations of unresolved subgrid-scale processes. The performance skill of the MME is generally higher than that of the constituent individual models. A number of meteorological/ climate prediction centers worldwide now operationally implement dynamical MME seasonal prediction routinely (Alves et al. 2003; Palmer et al. 2004; Saha et al. 2006; Lee et al. 2009). However, Lee et al. (2011) found that for some seasons and regions, the MME prediction skills are relatively limited. For its potential improvement, they introduced the novel concept of a ''climate filter,'' which is based on the relative reproducibility of a realistic climatic phenomenon. Specifically, Lee et al. (2011) diagnosed the fidelity of various Asia-Pacific Economic Cooperation (APEC) Climate Center (APCC) models in reproducing the strong observed relationship

Corresponding author address: Doo Young Lee, 12 Centum 7-ro, Haeundae-gu, Busan 612-020, South Korea.
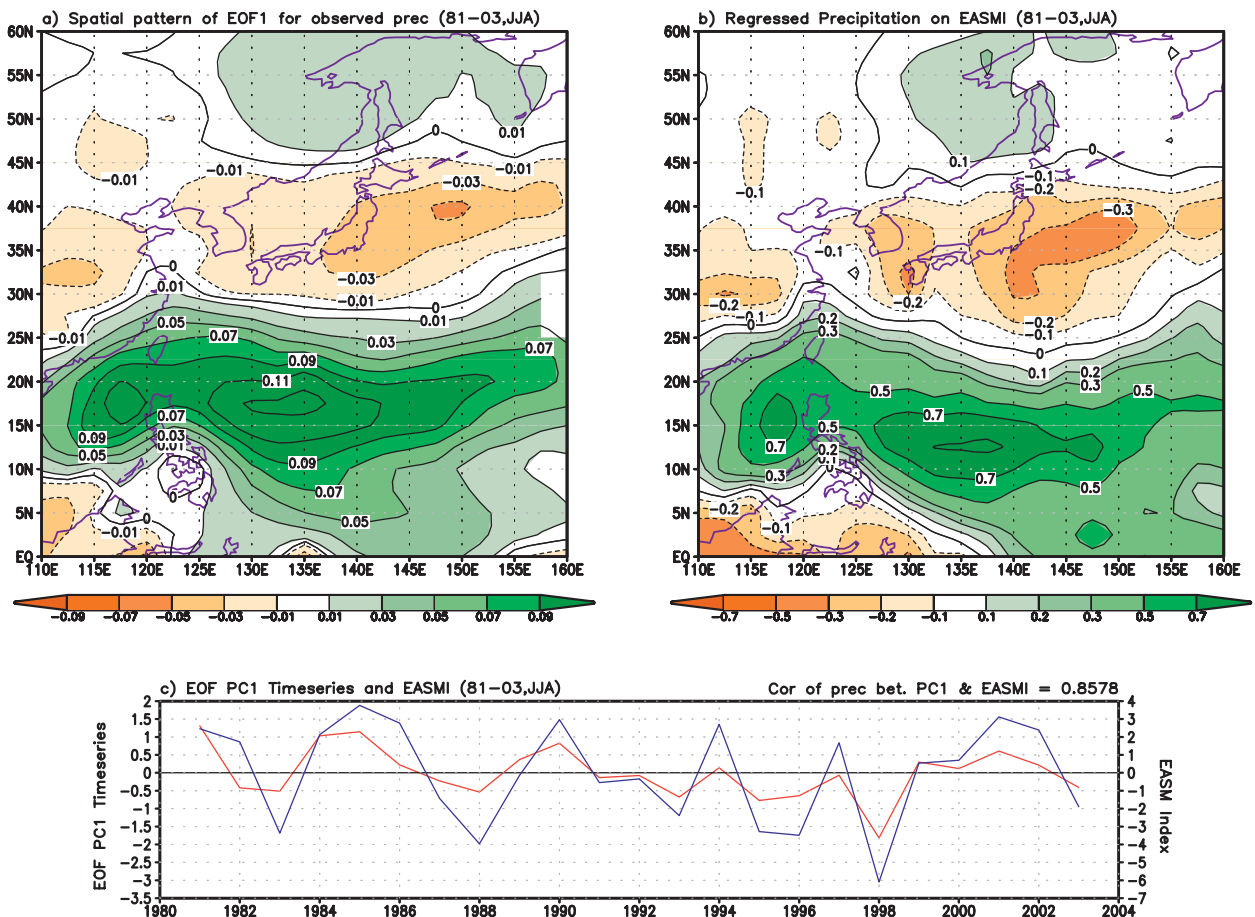E-mail: dylee@apcc21.org

FIG. 1. The distribution of (a) the spatial pattern of the first EOF mode for the observed precipitation and (b) regressed precipitation pattern on the WF index as an EASMI. (c) The corresponding principal component time series for observed precipitation (red line) and time series of EASMI (blue line). Temporal correlation between the first PC time series of the observed precipitation and EASMI is also given in the upper right.

between rainfall in the tropical Pacific Ocean and the local ENSO-associated Walker circulation during boreal winter. They noted that a newer MME with only the skillful models will improve the prediction skill of ENSO teleconnection for the regions abutting the western tropical Pacific, such as East Asia, the western North Pacific, and Australia, in contrast to an all model-inclusive MME or the individual models themselves. The study hints that models using the climate filter may provide appropriate heat sources in the tropics, which facilitate better teleconnection to the extratropics and beyond. Encouraged by the above study, we now wish to explore the potential of the aforementioned technique to improve the EASM rainfall prediction. We find that it is difficult to grade the models as more or less skillful, however, simply based on the relationship between the ENSO-associated Walker circulation and tropical Pacific rainfall for the boreal summer season, especially over the East Asian summer monsoon region (60°N–0°, 110°–160°E). The choice of this specific region for our study is explained in section 2c.

Important is that the EASM is influenced by the climate dynamics of the midlatitudes as well as by the large-scale tropical circulation, in addition to ENSO (Wang et al. 2008b; Lee et al. 2005; Wu et al. 2009; Gong et al. 2011; Gu et al. 2009), and has complex spatial and temporal structures. It is therefore imperative to identify various other relevant and significant climate drivers, whose individual or combined reproducibility will improve the prediction skills of the East Asian summer monsoon rainfall. It will also be useful to evaluate which of the available various EASM indices are more suitable as a predictor for the set of models.

The goal of the current study is to develop and facilitate the use of an expanded climate filter method to design a more effective MME suite for better predicting the EASM. The next section describes the observational and model data used, the various EASM indices (EASMIs) investigated, and the most important potential climate drivers in predicting the EASM variations. The section also introduces a multiclimate driver-based climate filter to rank

TABLE 1. Descriptions of the individual models used. Here POAMA is the Predictive Ocean–Atmosphere Model for Australia, GEM is the Global Environmental Multiscale Model, GM2 and GM3 are the second- and third-generation atmospheric general circulation models of the Canadian Centre for Climate Modelling and Analysis, SEF is Spectral aux Éléments Finis, GCPS is the Global Climate Prediction System, and GDAPS is the Global Data Assimilation and Prediction System.

Member economies	Acronym for models	Organization	Model resolution
Australia	POAMA	Bureau of Meteorology Research Centre	T47L17
Canada	MSC_GEM	Meteorological Service of Canada	$2° \times 2°$ L50
	MSC_GM2		T32L10
	MSC_GM3		T63L32
	MSC_SEF		T95L27
Taiwan	CWB	Central Weather Bureau	T42L18
South Korea	GCPS	Seoul National University	T63L21
	GDAPS_F	Korea Meteorological Administration	T106L21
	NIMR	National Institute of Meteorological Research	$5° \times 4°$ L17
United States	NCEP	National Centers for Environmental Prediction	T62L64

the individual models. In section 3, the relative performances of the various MMEs in terms of hindcast and forecast skills are presented. The summary and conclusions of the study can be found in section 4.

2. Design of the climate filter and the datasets used

a. Data used

Hindcast outputs for the period of 1981–2003 from 10 seasonal prediction models, which make up a major part of the operational MME for the APCC, have been used in the present study. The selection of these models is based on availability of the longest and most continuous quality-controlled common hindcast datasets. The description of the models is presented in Table 1. In addition, the National Centers for Environmental Prediction (NCEP)–U.S. Department of Energy (DOE) reanalysis 2 (Kanamitsu et al. 2002), and the Climate Prediction Center Merged Analysis of Precipitation (CMAP) (Xie and Arkin 1997) for the boreal summer seasons [June–August (JJA)] are used for the same period as observations for general circulation and rainfall. We also use the monthly-average global sea ice and sea surface temperature (GISST) version-2.2 (Rayner et al. 1996) datasets, and optimum interpolation SST (OISST) version-2 (Reynolds et al. 2002) datasets.

We adopt a simple composite MME method (Peng et al. 2002; Kang et al. 2009; Lee et al. 2008, 2009, 2011), which assigns equal weights to the ensemble mean predictions of individual models. The performance of this method is on par with the best available operational MME techniques (Lee et al. 2009). Henceforth, the term "MME" refers to this simple composite method, unless otherwise specified. The MME results are generated by the application of a bias correction (Lee et al. 2009, 2011) to model forecast anomalies, which are obtained from the standard "leave-one-out" cross-validation method (Michaelsen 1987; Jolliffe and Stephenson 2003; World Meteorological

Organization 2006; Kang et al. 2009). This cross-validation method essentially computes seasonal anomalies for each model parameter, from the corresponding yearly climatological means obtained by excluding information from the target year, as well as those of observations.

Finally, to explore its practical utility, the new methodology is applied in forecast mode to predict the EASM signals during the two boreal summer seasons of JJA 2009 and JJA 2010, for which forecast data from each of the participant models are available.

b. Comparison of the EASM indices and identification of important drivers

A climate filter involves the selection of better models based on the reproducibility of an observed physical relationship relevant to the region of interest—in this case, the EASM region. In addition, given that models are not always successful in simulating EASM rainfall variability, an efficient measure of model selection entails identification of a good dynamical–physical monsoon index from a choice of candidates, for which models are able to show improved simulation. Such an index should, of course, provide a succinct description of the EASM circulation variability on a broad scale. In addition, to focus in on the physical relationships that form the filter [e.g., ENSO-related Walker circulation in the case of winter tropical Pacific rainfall prediction, proposed by Lee et al. (2009)], as required in the current study, we explore the influence of various external climate phenomena in driving index form[1] and affecting EASM climate variability. These large-scale climate variations, such as ENSO and the

---

[1] A climate index is defined as a calculated value that can be used to describe the state and changes in the climate system. In this study, the climate drivers mean climate indices for large-scale climate variations influencing not only the EASM but also the global climate. They are largely independent of EASM variability in terms of their own interannual variation and evolution.

North Atlantic Oscillation (NAO), are the driving forces behind the climate variability not only in the EASM, but also across many regions of the globe.

We briefly introduce below the four dynamical EASM circulation indices (Wang and Fan 1999; Huang 2004; Zhang et al. 2003; Wang et al. 2001) that we consider in this study. We also introduce the four important climate drivers whose significant impacts on the EASM have been documented (Wang et al. 2008b; Li and Wang 2003; Wu et al. 2009; Thompson and Wallace 1998; Gong et al. 2011; Gu et al. 2009).

1) EAST ASIAN SUMMER MONSOON INDICES

The four dynamical EASM circulation indices are described in this section, along with their equations.

(i) The Wang and Fan index (Wang and Fan 1999; henceforth, the WF index) is defined as the difference of the area-averaged zonal wind at 850 hPa (U850) between two boxes:

$$WF = U850_{(5°-15°N,90°-130°E)} \\ - U850_{(22.5°-32.5°N,110°-140°E)}. \quad (1)$$

This index was designed to quantify the variability of the western North Pacific (WNP) summer monsoon circulation. This index reflects the relative variations in both the WNP monsoon trough and subtropical high; it is known that the two subsystems are the key elements of the EASM circulation system (Tao and Chen 1987). This index provides a useful measure of the subtropical and extratropical EASM (Wang et al. 2008b).

(ii) The East Asia–Pacific index of Huang (2004; hereinafter EAP index) is defined as follows:

$$EAP = -0.25Z'_{s(60°N,125°E)} + 0.50Z'_{s(40°N,125°E)} \\ - 0.25Z'_{s(20°N,125°E)}, \quad (2)$$

where $Z'_s = Z' \sin45°/\sin\varphi$ and represents the standardized seasonal mean 500-hPa height anomaly at a grid point provided in the associated parenthesis, with the latitude φ. The quantity Z' is the summer seasonal-mean 500-hPa height anomaly at the grid point. Previous studies (Huang and Sun 1992; Huang 2004) show that the EASM has a close relationship with the EAP teleconnection pattern.

(iii) The zonal wind difference index of Zhang et al. (2003; hereinafter the Zh index) is defined as the difference in the area-averaged U850 between two areas:

$$Zh = U850_{(10°-20°N,100°-150°E)} \\ - U850_{(25°-35°N,100°-150°E)}. \quad (3)$$

The index reflects the seesaw variation in convective intensity between the tropical monsoon trough and mei-yu front over the East Asia region (Zhang et al. 2003).

(iv) The meridional variation in the southerly component is an East Asian monsoon index defined by Wang et al. (2001) (hereinafter called the EAM index). This is defined as the difference between the JJA mean 850-hPa meridional wind anomalies averaged over the southern portion of the monsoon domain (20°–30°N, 110°–140°E) and those over the northern part (30°–40°N, 110°–140°E):

$$EAM = V850_{(20°-30°N,110°-140°E)} \\ - V850_{(30°-40°N,110°-140°E)}. \quad (4)$$

Wang et al. (2001) find that the index represents a delayed impact of El Niño on the East Asia summer monsoon because of the significant correlation between the summer EAM index and the preceding autumn Niño-3 SST anomaly (SSTA).

2) CLIMATE DRIVERS OF THE EAST ASIAN SUMMER MONSOON

In this work, we consider the following important climate drivers of the EASM as potential candidates for designing a climate filter to rank the individual model hindcasts.

(i) The first driver is the Niño-3.4 index in the previous winter. Wang et al. (2008b) find a strong and significant positive correlation between the first principal component (PC1) of EASM precipitation in JJA(0) and the Niño-3.4 index (seasonal SSTA area-averaged over 5°S–5°N, 170°–120°W) in the previous winter D(−1)JF(0). Based on this work, we identify the Niño-3.4 index during the preceding winter as representing a potential candidate for the design of the climate filter.

(ii) The second driver is the spring NAO anomaly. Wu et al. (2009) indicate that variability of the anomalous spring (April–May months, just prior to the summer season) NAO is tied to EASM variability. The NAO index is calculated as difference of the normalized monthly zonal-averaged sea level pressures (SLPs) over the longitudes of 80°W–30°E at the two latitude zones (35° and 65°N) (Li and Wang 2003; Wu et al. 2009).

(iii) The third driver is the Arctic Oscillation (AO) during the spring. A stronger-than-normal AO during the spring season (March–May) tends to enhance the horizontal wind shear at the 850-hPa level over

TABLE 2. Intertemporal correlation between various EASMIs. The asterisks and double asterisks mean that the skill scores are significant at the 99% and 95% confidence level from two-tailed Student's t test, respectively.

	EASMI (WF, JJA)	EASMI (EAP, JJA)	EASMI (Zh, JJA)	EASMI (EAM, JJA)
EASMI (WF, JJA)		0.59*	0.95*	−0.73*
EASMI (EAP, JJA)	0.59*		0.63*	−0.43**
EASMI (Zh, JJA)	0.95*	0.63*		−0.78*
EASMI (EAM, JJA)	−0.73*	−0.43**	−0.78*	

TABLE 3. Temporal correlation between various EASMIs and impacts related to EASM. The a, b, and c superscripts indicate that the skill scores are significant at the 99%, 95%, and 90%, confidence level from two-tailed Student's t test, respectively. DJF = December–February; AM = April–May; MAM = March–May.

	Niño-3.4 (previous DJF)	NAOI (AM)	AOI (MAM)	I_{NA} (previous DJF)
EASMI (WF, JJA)	−0.61[a]	0.45[b]	−0.39[c]	0.08
EASMI (EAP, JJA)	−0.55[a]	0.09	0.08	0.13
EASMI (Zh, JJA)	−0.70[a]	0.30	−0.30	0.15
EASMI (EAM, JJA)	0.49[b]	−0.13	0.32	0.15

East Asia in the following summer. This, in turn, tends to enhance the rainfall (Gong et al. 2011). Following Thompson and Wallace (1998) and Gong et al. (2011), we compute the AO index (AOI) for the spring months as the principal component associated with the first empirical orthogonal function (EOF) of the monthly SLP north of 20°N.

(iv) The fourth driver is the preceding winter North Atlantic SSTA. Gu et al. (2009) find that the wintertime North Atlantic SSTA could exert a delayed impact on East Asian circulation in the following summer. North Atlantic SSTA is strongly correlated with mei-yu rainfall. Following Gu et al. (2009), we compute the North Atlantic SSTA index (I_{NA}) as the difference between the normalized area-averaged SSTA for 40°–55°N, 30°–15°W and 25°–35°N, 75°–60°W.

3) RELATIONSHIP BETWEEN EASM INDICES AND DRIVERS OF THE EASM

To confirm agreement between the four EASM indices discussed above, we present the temporal intercorrelation coefficients between individual EASM indices for the study period of 1981–2003 (Table 2). As expected, these are highly correlated with one another, and are significant, above 95% confidence level from a two-tailed Student's t test. This means that any of these indices can be used to monitor and predict EASM variability.

Table 3 catalogs the correlations between the various EASM indices and the EASM drivers, listed in subsection 2b above. It can be discerned that most of the EASM indices shown have significant correlations (−0.61, −0.55, −0.70, and 0.49) with the previous winter Niño-3.4 index, indicating that the ENSO signal during the preceding winter is an important contributor to the interannual variability of the EASM. However, the preceding winter I_{NA} index shows a relatively poor relationship with the EASM indices. We also find that the

spring NAO index has a statistically significant and strong correlation with only the WF index as opposed to all EASM indices.

It can be seen that the WF index, among all the EASM indices, displays the strongest correlations with the majority of the drivers. In particular, it is very closely related to the observed ENSO and NAO forcings. In addition, there is no apparent strong relationship between the indices of the preceding winter Niño-3.4 and the spring NAO (figure not shown), suggesting that they cannot be independent predictors for the EASM variability.

Based on these results, we decide to use the WF index as the primary EASM index in this work. To justify this, we present the EASM precipitation regressed onto the WF index (Fig. 1b). Both Figs. 1a and 1b show a meridional tripole structure that are similar to one another, confirming the suitability of the WF index in representing the EASM variability. We particularly note a continuous zonal band covering eastern China, the Korean Peninsula, Japan, and eastward, with opposite signatures over the South China Sea, the western Pacific including the Philippine Sea to the south, and over the vicinity of the Okhotsk Sea to the north (Figs. 1a,b). The pattern reminds us of the well-known Pacific–Japan pattern proposed by Nitta (1987). The time series of the corresponding principal components for the observed EASM precipitation and WF index are shown in Fig. 1c. These are very strongly correlated at 0.86, and the pattern correlation between the distributions shown in Figs. 1a and 1b amounts to 0.85.

Further, we propose to utilize the preceding winter Niño-3.4 and the spring NAO indices, as the drivers from the tropics and midlatitudes, respectively (Wu et al. 2009), to design a climate filter.

c. Climate filter to predict the EASM rainfall

In the preceding sections, we established the appropriateness of the WF index to represent the interannual
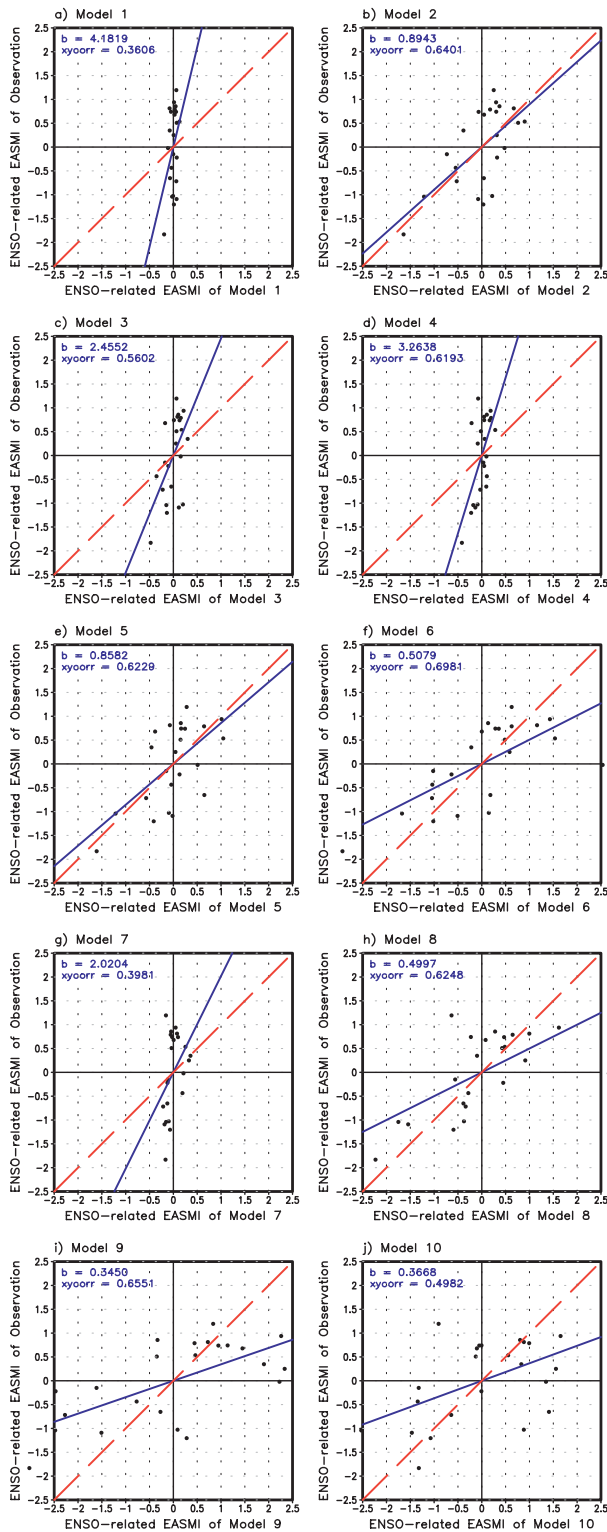
FIG. 2. The ENSO-associated EASMI defined by the U850 in (5°–15°N, 90°–130°E) minus U850 in (22.5°–32.5°N, 110°–140°E) from observation (*y* axis), for 23 boreal summers in the period of 1981–2003, plotted against those from the individual models (*x* axis) for models 1–10. The blue solid line is the statistical line of fit, and the red dashed line is a reference diagonal line. The slope *b* from the regression line of fit is provided in the upper left. The term xycorr stands for the temporal correlations between the observation and each model.

variability of the EASM. We have also identified the spring NAO index (NAOI) and previous winter Niño-3.4 index as the best-linked indices representing important climate drivers of EASM variability. From Figs. 1a and 1b, we can also accept that the region 60°N–0°, 110°–160°E can designate the East Asia summer monsoon area and a close relationship between monsoon rainfall and EASM index over the EASM region is observed. This work suggests that reproducibility of the observed relationships between the East Asian monsoon circulation and the preceding winter ENSO and/or spring NAO impact will be important minimum requirements for any model possessing the necessary fidelity. Therefore, we use these two conditions as a basis to design a climate filter to classify the individual constituent models.

Specifically, following the general methodology of Lee et al. (2011), we carry out the following computations:

(i) We utilize the observed preceding winter Niño-3.4 index and the spring NAO index as weights to compute the ENSO-associated EASMI and NAO-associated EASMI in the models.

(ii) We then obtain the squared partial correlation coefficient between the WF index, and the preceding winter Niño-3.4 index, adjusted for spring NAO, subsequently obtaining the squared partial correlation coefficient between the WF index and spring NAO, after separating out any impact from the preceding winter Niño-3.4. As is known, the squared correlation coefficient describes the fraction of variance in common between the two variables and is one of the best means for evaluating the strength of a linear association between *x* and *y* (Wilks 1995; Spiegel and Stephens 2008); it is widely used in climate studies and applications (Nicholls 1989; Ashok et al. 2003, 2007, 2009; Saji and Yamagata 2003, etc.). From this point, the computed squared correlation coefficient between the WF index and spring NAO/previous winter Niño-3.4 index is used as an appropriate weight representing the variance of EASMI associated with the spring NAO index/previous winter Niño-3.4 index.

(iii) In the next step, we carry out a scatter diagram analysis to identify the models that capture the
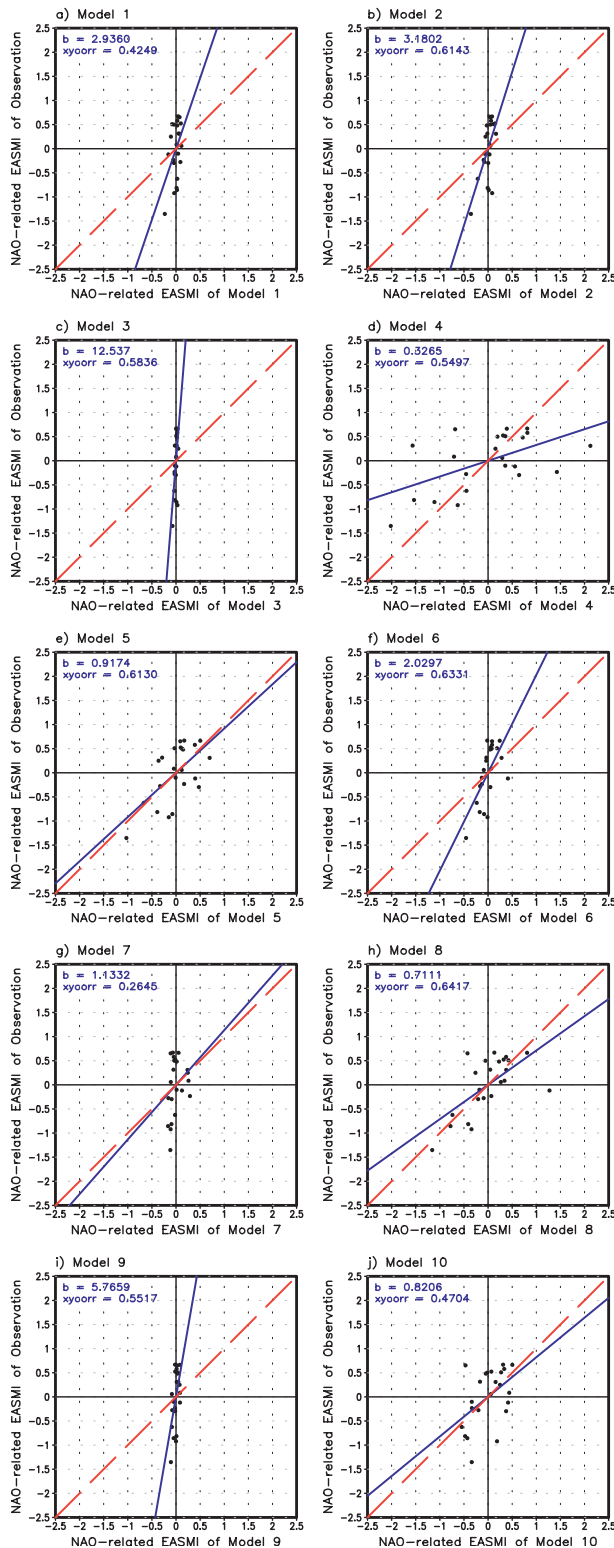
FIG. 3. As in Fig. 2, but for the NAO-associated EASMI.

variability associated with the previous winter ENSO, and that of the spring NAO. Then, we compute the local ENSO- and NAO-associated EASMI applying the aforementioned weights from observations for the 23 boreal summers during the study period of 1981–2003. The ENSO- and NAO-associated EASM indices are also computed for each model from hindcast data for the same period. The observed previous winter ENSO- and spring-NAO-associated EASM index is plotted separately against those from individual models. The reproduction of both the associations, subject to some objective conditions described in the next paragraph, forms our proposed climate filter that would distinguish the most skillful models.

We have used two objective conditions defined by Lee et al. (2011) to identify the skillful models. These two criteria are (i) that the slope of the fit between the observed and predicted EASM index should be greater than 0.5 and less than 1.5, and (ii) that the temporal correlation coefficient between two indices is more than 0.4, the statistically significant value at the 90% confidence level from a two-tailed Student's t test for the period of 1981–2003.

In this study, we employ the Student's two-tailed t test (Wilks 1995; Spiegel and Stephens 2008) to evaluate significance levels. While applying this test to temporal correlations, we compute the statistical significance using the simple number of degrees of freedom, while for the spatial pattern correlations we applied the effective spatial degree of freedom (ESDOF) criterion (Snedecor and Cochran 1980; Bretherton et al. 1999; Wang and Shen 1999). Finally, while applying the climate filter to model selection for the study period of 1981–2003, we use the leave-one-out cross validation (Michaelsen 1987; Jolliffe and Stephenson 2003; World Meterological Organization 2006; Kang et al. 2009) in each target year to examine the selection of models.

3. Evaluation of the hindcast relationship through the climate filter method

Figures 2 and 3 show the scatter diagrams illustrating the reproducibility of EASM indices influenced by the previous winter Niño-3.4 and spring NAO impacts, respectively. Applying the two objective conditions mentioned above, we found that only 5 out of the 10 models passed. For convenience, we group the five better-performing models, which successfully reproduced the observed association with ENSO during previous winter, and the spring NAO, as class A models (models 2, 5, 6, 8, and 10). The remaining models are grouped as class B (models 1, 3, 4, 7, and 9).
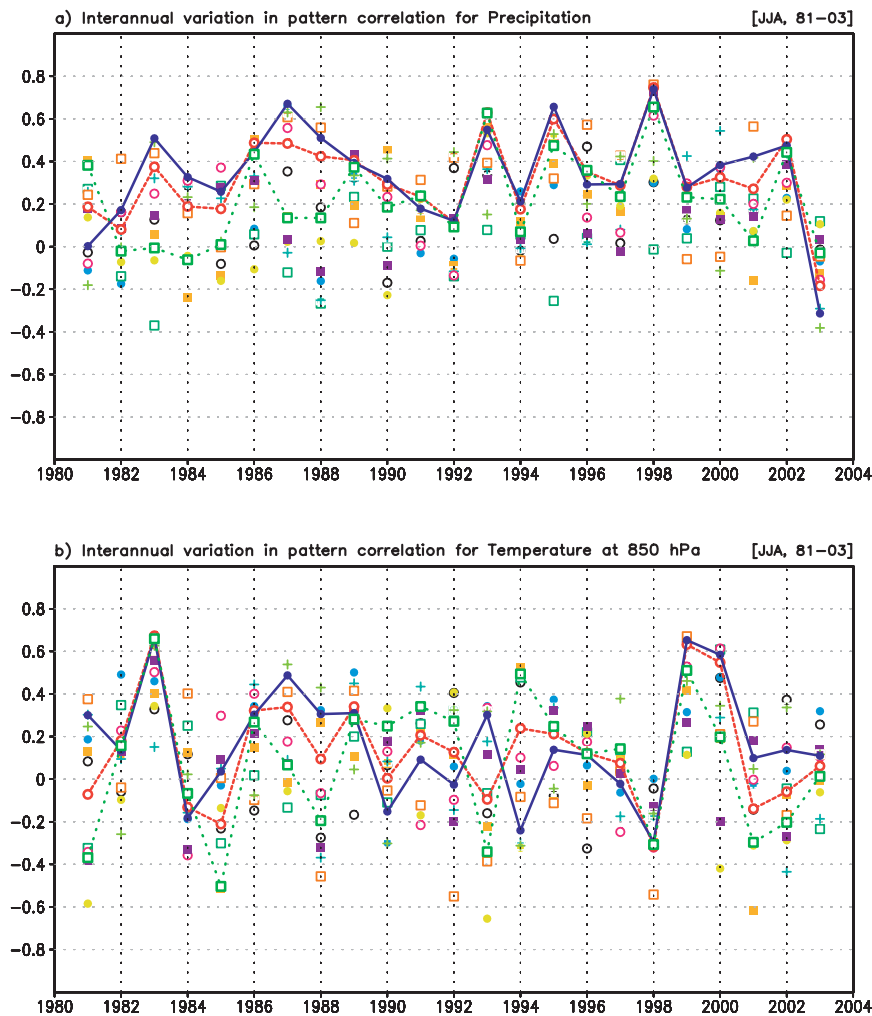
FIG. 4. Time series of the spatial pattern correlations between the observed and the predicted (a) precipitation from M10 (dashed red line), A5 (solid blue line), B5 (dotted green line), and individual models (colored symbols) over the East Asian summer monsoon (60°N–0°, 110°–160°E) region. M10, A5, and B5 are the multimodel ensemble predictions based on a simple composite method using the total of 10 models, the 5 more skillful models, and the 5 less skillful models, respectively. (b) As in (a), but for the 850-hPa temperature.

Next, following Lee et al. (2011), three separate MME hindcast experiments have been carried out, which are named as the A5 experiment (based on the hindcasts from the class A models), the B5 experiment (uses the hindcasts from the class B models), and the M10 experiment (uses the hindcasts from all 10 models). The time series of the spatial pattern correlations between the observed and hindcast rainfall from all three MME experiments and individual models over the East Asian summer monsoon region are shown in Fig. 4a, and the corresponding results for the 850-hPa temperature in Fig. 4b. In general, it can be discerned that the prediction skills of the MME are superior to those of individual models. Notwithstanding an apparent uniform

level of skills across a few years, we find significant differences in the prediction skills, as shown in Table 4. Especially, it is notable that the 0.34 skill score of the A5 experiment (significant at 85% confidence level from two-tailed Student's t test; ESDOF = 16.6) for the rainfall is significantly higher than the corresponding skill score of 0.23 from the B5 experiment (significant at 70% confidence level from two-tailed Student's t test; ESDOF = 21.3) in Fig. 4a, and betters the skill (0.32) from the M10 experiment (significant at 85% confidence level from the two-tailed t test; ESDOF = 20.3). In addition, we can see that the time averaged MME prediction skills for precipitation are slightly higher than those for temperature at 850 hPa in Table 4.

TABLE 4. Time average of the spatial pattern correlations between the observation and various multimodel ensemble hindcast experiments (M10, A5, and B5) for precipitation and temperature at 850 hPa over the EASM (60°N–0°, 110°–160°E) region. M10, A5, and B5 comprise all 10 models, the 5 more skillful models, and the 5 less skillful models, respectively.

Variables	Correlations		
	M10	A5	B5
Precipitation	0.323	0.343	0.226
850-hPa temperature	0.137	0.167	0.075

To further clarify the significance of the performance of the three types of MME for precipitation, we also carry out a significance test using a ranking distribution of a time-averaged pattern correlation for various five-model combinations using independent possible choices of five models from all the given 10 models (10C5) equaling 252 combinations (see Fig. 5). After counting the number of combinations that have skills equal to or higher than the MME-predicted skill for each experiment respectively, the ratios of the counted number to the total number of combinations are calculated (Wilks 1995; Tanizaki 2006). It is apparent that the A5 MME prediction skill (14/252, significant at 94.44% confidence level) is superior not only to the B5 MME prediction skill (249/252, significant at the 1.19% confidence level) but also to the M10 MME skill (54/252, significant at 78.57% confidence level).

To investigate the spatial distribution of prediction skills of all the MMEs for precipitation and temperature at 850 hPa, we present the relevant temporal correlation coefficients for the period of 1981–2003 in Fig. 6. It is clear that over the whole East Asian summer monsoon region, the prediction skills (domain-averaged skills for rainfall and temperature are 0.262 and 0.350 respectively) of the A5 experiment are significantly better than those (0.172 and 0.269) of B5 for both variables, and somewhat better than the skills (0.248 and 0.333) from M10.

However, we find that the MME prediction skills for precipitation are poor and insignificant over several land areas. Primarily, it can be found that the overall rainfall performances of individual models are relatively poor over the land area in comparison with those over the ocean (figure and table not shown). This fact suggests that performance enhancement of the individual models should be a fundamental basis for overcoming the limitations of the MME seasonal prediction.

We have applied the climate filter method to real-time forecasts to assess the potential usefulness of this method. The MME forecast dataset for the two boreal summer seasons from June to August 2009 and from June to August 2010 over the East Asia summer monsoon
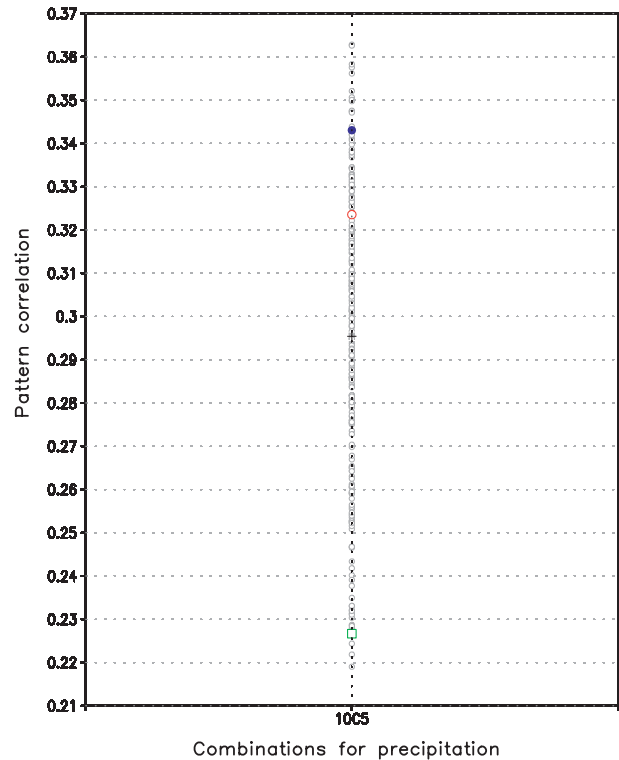

FIG. 5. A time average of spatial pattern correlations between the observed and the MME-predicted precipitations, which are computed by 5-model combinations using independent possible choice of 5 models (10C5 = 252) from the original 10 models, over the East Asia summer monsoon region. The gray circles show the prediction skills of 252 total combinations. The red open circle, blue filled circle, and green square indicate MME prediction skills using the total of 10 models (M10), the 5 more skillful models (A5), and the 5 less skillful models (B5), respectively. The black plus sign indicates the averaged skill of the total combinations.

(110°–160°E and 0°–60°N) region are used. The spatial pattern correlations for rainfall and 850-hPa temperature are depicted in Fig. 7. The A5 MME prediction skills for two variables (precipitation of 2009 and temperature of 2010) are better than those of both the all model-inclusive M10 and B5 MMEs. However, all the MME experiments indicate the insignificant skill scores for the anomalous 2009 temperature and 2010 rainfall distribution, the reasons for which need to be examined further.

4. Summary and conclusions

We propose and demonstrate a new approach to enhancing MME prediction skill for EASM rainfall and 850-hPa temperature by evaluating the relative capabilities of a suite of models to reproduce the association of the EASM variability with a few relevant climate drivers for the period 1981–2003. The NCEP–DOE reanalysis 2 (Kanamitsu et al. 2002), CMAP rainfall (Xie
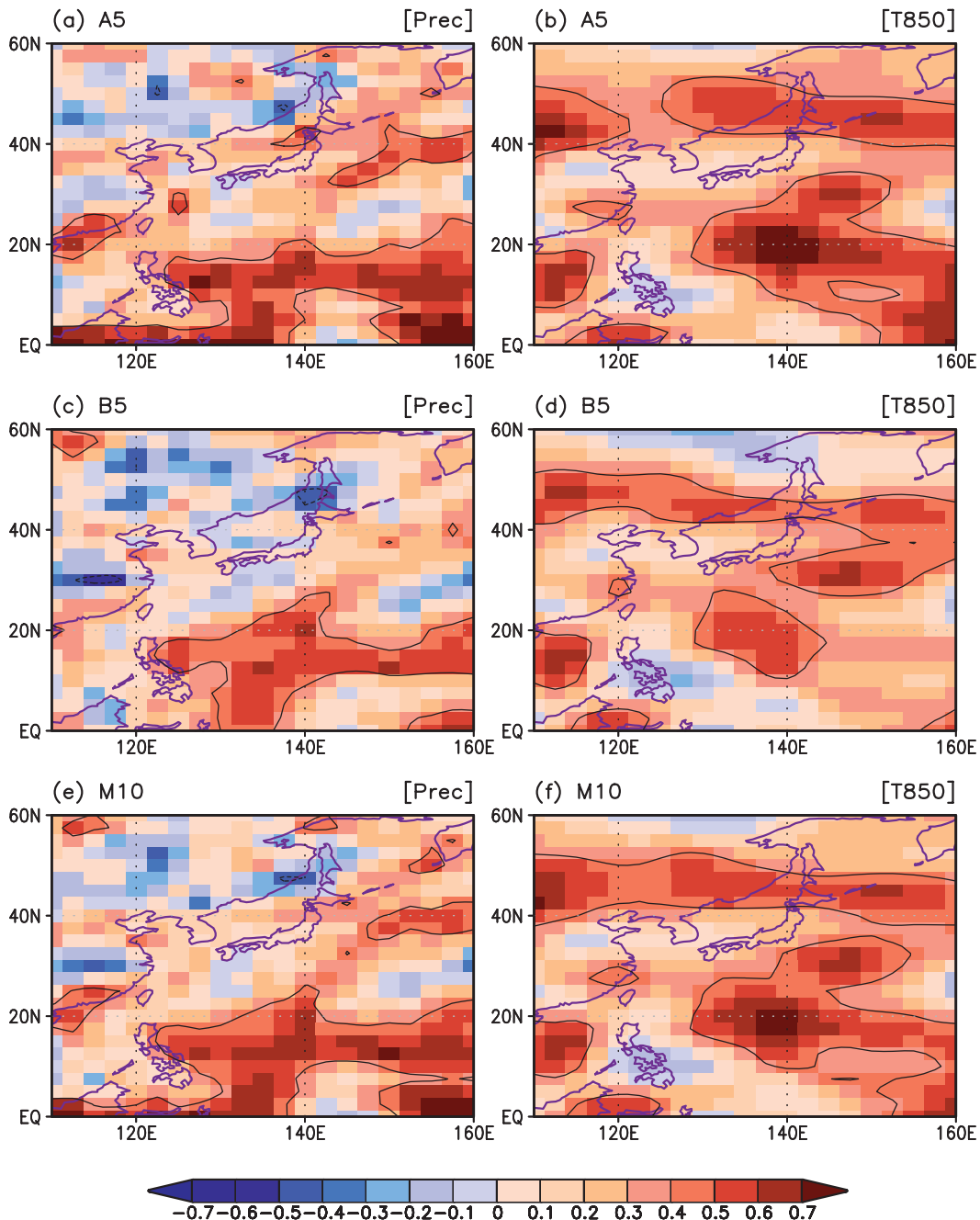
FIG. 6. Temporal correlation coefficients between the observed and predicted (left) precipitation and (right) temperatures at 850 hPa from (a),(b) A5, (c),(d) B5, and (e),(f) M10. The contour line depicts the region of significant correlation (0.413) at the 95% confidence level from a two-tailed Student's t test.

and Arkin 1997), SST datasets from GISST 2.2 (Rayner et al. 1996) and OISST v2 (Reynolds et al. 2002), and APCC operational MME hindcast datasets are used in this study. The EASM is subject to complex variability, spatial and temporal structures, and is not only influenced by climate variations originating in the tropics but also by those from midlatitudes. We identified the

observed WF (Wang and Fan 1999) as the most suitable EASM variability index in this study. Further, through a diagnostic analysis, we identified two major climate drivers, namely the previous winter Niño-3.4 index (Wang et al. 2008b) and spring NAO index (Li and Wang 2003), as the most suitable drivers of EASM climate, which may be used to design a climate filter to grade model
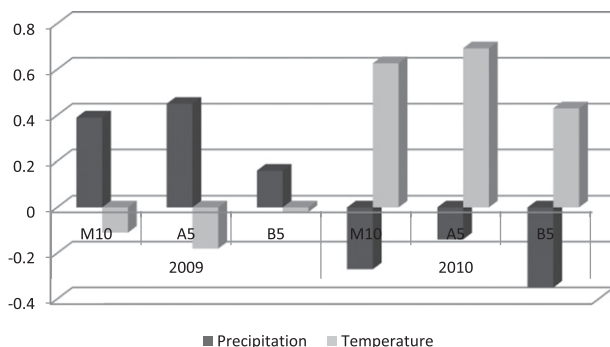
FIG. 7. Spatial pattern correlations between the observed and predicted precipitation (dark-shaded bars), and temperature at 850 hPa (light-shaded bars) for two boreal summer seasons of JJA 2009 and JJA 2010 over the EASM (60°N–0°, 110°–160°E) region.

performances. We graded the models based on the degree of reproducibility of the association of EASM variability and the aforementioned climate drivers in the respective model hindcasts. It can be seen that the MME hindcast skills from five better-performing models are significantly higher in retrospective prediction of the EASM variability, compared to those from an MME with the rest of the nonperforming models, and also from an all-inclusive 10-model MME. However, the relatively small size of available hindcast and forecast datasets poses a sampling limitation, particularly in the forecast cases. Nonetheless, this research, built on the earlier work by Lee et al. (2011), indicates that the MME is better skilled if models that can reproduce observed response to major drivers are used.

REFERENCES

Alves, O., and Coauthors, 2003: POAMA: Bureau of Meteorology operational coupled model seasonal forecast system. *Proc. National Drought Forum,* Brisbane, Australia, Queensland Dept. of Primary Industries, 49–56.

Ashok, K., Z. Guan, and T. Yamagata, 2003: Influence of the Indian Ocean dipole on the Australian winter rainfall. *Geophys. Res. Lett.,* **30,** 1821, doi:10.1029/2003GL017926.

——, S. K. Behera, S. A. Rao, H. Weng, and T. Yamagata, 2007: El Niño Modoki and its possible teleconnection. *J. Geophys. Res.,* **112,** C11007, doi:10.1029/2006JC003798.

——, C.-Y. Tam, and W.-J. Lee, 2009: ENSO Modoki impact on the Southern Hemisphere storm track activity during extended austral winter. *Geophys. Res. Lett.,* **36,** L12705, doi:10.1029/2009GL038847.

Barnston, A. G., S. J. Mason, L. Goddard, D. G. Dewitt, and S. E. Zebiak, 2003: Multimodel ensembling in seasonal climate forecasting at IRI. *Bull. Amer. Meteor. Soc.,* **84,** 1783–1796.

Bretherton, C., M. Widmann, V. Dymnikov, J. Wallace, and I. Blade, 1999: The effective number of spatial degrees of freedom of a time-varying field. *J. Climate,* **12,** 1990–2009.

Ding, Y., and J. C. L. Chan, 2005: The East Asia summer monsoon: An overview. *Meteor. Atmos. Phys.,* **89,** 117–142.

Doblas-Reyes, F. J., M. Deque, and J.-P. Piedelievre, 2000: Multimodel spread and probabilistic seasonal forecasts in PROVOST. *Quart. J. Roy. Meteor. Soc.,* **126,** 2069–2088.

——, R. Hagedorn, and T. N. Palmer, 2005: The rationale behind the success of multi-model ensembles in seasonal forecasting—II. Calibration and combination. *Tellus,* **57A,** 234–252.

Gong, D. Y., J. Yang, S. J. Kim, Y. Q. Gao, D. Guo, T. J. Zhou, and M. Hu, 2011: Spring Arctic oscillation-East Asian summer monsoon connection through circulation changes over the western North Pacific. *Climate Dyn.,* **37,** 2199–2216, doi:10.1007/s00382-011-1041-1.

Gu, W., C. Y. Li, X. Wang, and W. Zhou, 2009: Linkage between Meiyu precipitation and North Atlantic SST on the decadal timescale. *Adv. Atmos. Sci.,* **26,** 101–108, doi:10.1007/s00376-009-0101-5.

Hagedorn, R., F. J. Doblas-Reyes, and T. N. Palmer, 2005: The rationale behind the success of multi-model ensembles in seasonal forecasting—I. Basic concept. *Tellus,* **57A,** 219–233.

Huang, G., 2004: An index measuring the interannual variation of the East Asian summer monsoon—The EAP index. *Adv. Atmos. Sci.,* **21,** 41–52.

Huang, R., and F. Sun, 1992: Impacts of the tropical western Pacific on the East Asia summer monsoon. *J. Meteor. Soc. Japan,* **70,** 243–256.

Jolliffe, I. T., and D. B. Stephenson, 2003: *Forecast Verification: A Practitioner's Guide in Atmospheric Science.* John Wiley and Sons, 254 pp.

Kanamitsu, M., and Coauthors, 2002: NCEP–DOE AMIP-II Reanalysis (R-2). *Bull. Amer. Meteor. Soc.,* **83,** 1631–1643.

Kang, H., and Coauthors, 2009: Statistical downscaling of precipitation in Korea using multimodel output variables as predictors. *Mon. Wea. Rev.,* **137,** 1928–1938.

Krishnamurti, T. N., and Coauthors, 1999: Improved weather and seasonal climate forecasts from multimodel superensemble. *Science,* **285,** 1548–1550.

——, C. M. Kishtawal, D. W. Shin, and C. E. Williford, 2000: Multimodel superensemble forecasts for weather and seasonal climate. *J. Climate,* **13,** 4196–4216.

Lee, D. Y., C.-Y. Tam, and C.-K. Park, 2008: Effects of multicumulus convective ensemble on East Asian summer monsoon rainfall simulation. *J. Geophys. Res.,* **113,** D24111, doi:10.1029/2008JD009847.

——, K. Ashok, and J.-B. Ahn, 2011: Toward enhancement of prediction skills of multimodel ensemble seasonal prediction: A climate filter concept. *J. Geophys. Res.,* **116,** D06116, doi:10.1029/2010JD014610.

Lee, E.-J., J.-G. Jhun, and C.-K. Park, 2005: Remote connection of the northeast Asian summer rainfall variation revealed by a newly defined monsoon index. *J. Climate,* **18,** 4381–4393.

Lee, W.-J., and Coauthors, cited 2009: APEC Climate Center for Climate Information Services, APCC 2009 Final Rep. [Available online at http://www.apcc21.net/eng/research/pub/repo/japcc040602_lst.jsp.]

Li, J., and J. Wang, 2003: A new North Atlantic oscillation index and its variability. *Adv. Atmos. Sci.,* **20,** 661–676.

Michaelsen, J., 1987: Cross-validation in statistical climate forecast models. *J. Climate Appl. Meteor.,* **26,** 1589–1600.

Nicholls, N., 1989: Sea surface temperatures and Australian winter rainfall. *J. Climate,* **2,** 965–973.

Nitta, T., 1987: Convective activities in the tropical western Pacific and their impact on the Northern Hemisphere summer circulation. *J. Meteor. Soc. Japan,* **65,** 373–390.

Palmer, T. N., C. Brankovic, and D. S. Richardson, 2000: A probability and decision-model analysis of PROBOST seasonal multi-model ensemble integrations. *Quart. J. Roy. Meteor. Soc.,* **126,** 2013–2034.

——, and Coauthors, 2004: Development of a European Multi-model Ensemble System for Seasonal to Interannual Prediction (DEMETER). *Bull. Amer. Meteor. Soc.,* **85,** 853–872.

Peng, P., A. Kumar, H. van den Dool, and A. G. Barnston, 2002: An analysis of multimodel ensemble predictions for seasonal climate anomalies. *J. Geophys. Res.,* **107,** 4710, doi:10.1029/2002JD002712.

Rayner, N. A., E. B. Horton, D. E. Parker, C. K. Folland, and R. B. Hackett, 1996: Version 2.2 of the Global Sea Ice and Sea Surface Temperature data set, 1903–1994. Met Office Hadley Centre Climate Research Tech. Note CRTN74, 35 pp.

Reynolds, R. W., N. A. Rayner, T. M. Smith, D. C. Stokes, and W. Wang, 2002: An improved in situ and satellite SST analysis for climate. *J. Climate,* **15,** 1609–1625.

Saha, S., and Coauthors, 2006: The NCEP Climate Forecast System. *J. Climate,* **19,** 3483–3517.

Sahai, A. K., R. Chattopadhyay, and B. N. Goswami, 2008: A SST based large multi-model ensemble forecasting system for Indian summer monsoon rainfall. *Geophys. Res. Lett.,* **35,** L19705, doi:10.1029/2008GL035461.

Saji, N. H., and T. Yamagata, 2003: Structure of SST and surface wind variability during Indian Ocean dipole mode events: COADS observations. *J. Climate,* **16,** 2735–2751.

Shukla, J., and Coauthors, 2000: Dynamical seasonal prediction. *Bull. Amer. Meteor. Soc.,* **81,** 2593–2606.

Snedecor, G. W., and W. G. Cochran, 1980: *Statistical Methods.* 7th ed. Iowa State University Press, 507 pp.

Spiegel, M. R., and L. J. Stephens, 2008: *Schaum's Outline of Theory and Problems of Statistics.* 4th ed. McGraw-Hill, 577 pp.

Tanizaki, H., 2006: On small sample properties of permutation tests: A significance test for regression models. *Kobe Univ. Econ. Rev.,* **54,** 27–40.

Tao, S., and L.-X. Chen, 1987: A review of recent research on the East Asian summer monsoon in China. *Monsoon Meteorology,* C.-P. Chang and T. N. Krishnamurti, Eds., Oxford University Press, 60–92.

Thompson, D. W. J., and J. M. Wallace, 1998: The Arctic oscillation signature in the wintertime geopotential height and temperature fields. *Geophys. Res. Lett.,* **25,** 1297–1300.

Wang, B., and Z. Fan, 1999: Choice of south Asian summer monsoon indices. *Bull. Amer. Meteor. Soc.,* **80,** 629–638.

——, and Coauthors, 2008a: How accurately do coupled climate models predict the leading modes of Asian-Australian monsoon interannual variability? *Climate Dyn.,* **30,** 605–619.

——, Z. Wu, J. Li, J. Liu, C.-P. Chang, Y. Ding, and G. Wu, 2008b: How to measure the strength of the East Asian summer monsoon. *J. Climate,* **21,** 4449–4463.

——, and Coauthors, 2009: Advance and prospectus of seasonal prediction: Assessment of the APCC/CliPAS 14-model ensemble retrospective seasonal prediction (1980–2004). *Climate Dyn.,* **33,** 93–117.

Wang, X., and S. S. Shen, 1999: Estimation of spatial degrees of freedom of a climate field. *J. Climate,* **12,** 1280–1291.

Wang, Y. F., B. Wang, and J.-H. Oh, 2001: Impacts of the preceding El Niño on the East Asian summer atmospheric circulation. *J. Meteor. Soc. Japan,* **79,** 575–588.

Wilks, D. S., 1995: *Statistical Methods in the Atmospheric Sciences: An Introduction.* Academic Press, 467 pp.

World Meteorological Organization, 2006: Attachment II-8, Standardised Verification System (SVS) for Long-Range Forecasts (LRF). *Manual on the Global Data-Processing and Forecasting System: WMO-No. 485,* Vol. 1. WMO, II.8-1–II.8-17.

Wu, Z., B. Wang, J. Li, and F.-F. Jin, 2009: An empirical seasonal prediction model of the East Asian summer monsoon using ENSO and NAO. *J. Geophys. Res.,* **114,** D18120, doi:10.1029/2009JD011733.

Xie, P., and P. A. Arkin, 1997: Global precipitation: A 17-year monthly analysis based on gauge observations, satellite estimates, and numerical model outputs. *Bull. Amer. Meteor. Soc.,* **78,** 2539–2588.

Yun, W.-T., and Coauthors, 2005: A multi-model superensemble algorithm for seasonal climate prediction using DEMETER forecasts. *Tellus,* **57A,** 280–289.

Zhang, Q. Y., S. Y. Tao, and L. T. Chen, 2003: The interannual variability of East Asian summer monsoon indices and its association with the pattern of general circulation over East Asia (in Chinese). *Acta Meteor. Sin.,* **61,** 559–568.